ARM PROGRESS REPORT

1. PI and Co-I Names and Affiliations:

Principal Investigators: Catherine Gautier[1, 2] and Paul Ricchiazzi[1]
Co-Principal Investigators: William O'Hirok[1] and Klaus Wyser[1]
Collaborators: Charles Jones[1] and Allison Payton[1]
[1]ICESS, University of California, Santa Barbara
[2]Dept. of Geography, University of California, Santa Barbara

2. Title of Research Grant:

Effect of Cloudiness Heterogeneity on Radiative Budget at the Top of the Atmosphere and at the Surface: Modeling, Verification, and Analysis

3. Scientific Goals of Research Grant

The particular emphasis of our proposed research is on clouds and aerosol interaction with radiation using radiative transfer modeling and observational studies in support of process modeling and GCM Parameterization. The specific goals of this research are: 1) to analyze observations in conjunction with a variety of newly developed radiative transfer models to unravel the issue of solar radiation absorption by clear and cloudy atmosphere; 2) to enhance spectral resolution and accuracy of 1-D and 3-D radiative transfer models; 3) to understand the role of sub-grid scale cloud variability on GCM grid-scale radiative fluxes; 4) to develop new GCM parameterizations of cirrus cloud and aerosol effects on shortwave radiation for use in GCM and process models; 5) to analyze spectrally resolved data in conjunction with radiative transfer codes to quality control the data and evaluate the codes in particular spectral regions of interest (e.g., O_2-O_2 and water vapor absorption bands); and 6) to develop a framework for analysis of CART multiple surface observations and derive aerosol and cirrus properties from these observations.

4. Accomplishments

• **Investigations of 3-D cloud effects on atmospheric heating and cooling rates** – A 3-D radiative transfer model is used to compute both shortwave and longwave radiative fluxes and associated heating and cooling rates for a convective cloud field. Results show that sampled heating and cooling rate profiles are poorly characterized by the

domain average profile, and the use of domain averages or even highly resolved independent column approximations of the radiative fluxes cannot characterize the actual heating rate of a cloud field.

• **High resolution modeling of cloud fields at TWP site** – Comparison between modeled (MM5) and observed state of the atmosphere at the ARM TWP site at Nauru show that the model captures the mean state of the atmosphere but not the variability. It is likely that the problem is related to the external forcing and the domain size of the model. The microphysical schemes do not seem to affect the systematic difference found.

• **Interpretation of effect of surface albedo heterogeneity on sky radiance** - Observations of sky radiance with an all-sky camera and a narrow field-of-view spectrometer were made under clear and cloudy. The observed sky radiance distribution was found to roughly mirror the spatial distribution of surface albedo. Comparisons with computational results from a 3-D Monte-Carlo radiation model that explicitly includes the interaction of radiation with heterogeneous surface features show a good agreement.

• **Analysis of spectrally resolved spectrometer data in conjunction with RT model computations** – Spectral irradiance data obtained with Peter Pilewskie's solar spectral flux radiometer (SSFR) at the Surface Heat Budget of the Arctic (SHEBA) site were analyzed using SBMOD, our moderate resolution radiative transfer code. Though the analysis is still at a preliminary stage, modeled and observational results show close agreement, with the exception of a mid-visible "bulge" that may be due to the excess extra terrestrial solar input recently observed by Harrison.

5. Progress and accomplishments during last twelve months

During this first year, work has taken place in four different directions in accordance to our proposed goals: 1) the computations of high resolution heating rates in 3-D clouds, 2) the high resolution modeling of cloud fields at TWP site, 3) the interpretation of effect of surface albedo heterogeneity on sky radiance and 4) the analysis of spectrally resolved spectrometer data in conjunction with model computations. Much of the work is still preliminary but it generally suggests an excellent ability to model radiative transfer through the atmosphere even under complex surface and cloud conditions.

High resolution heating and cooling rates in 3-D Clouds (O'Hirok and Gautier)

In this study we examine how well the domain averaged heating and cooling rate profile represents the actual spatial variability of those quantities using a 3-D radiative transfer model. The input consists of a 2-D slice of a convective cloud field embedded in a tropical atmosphere (Fig 1). Shortwave fluxes were computed for solar zenith angles of 0, 41, 60 and 75 degrees.

For overhead sun in the shortwave, photon leakage from the higher portions of the cloud top combined with internal multiple scattering at cloud top troughs produce fluxes greater than the TOA input (Fig 2). For oblique solar zenith angles, the highest downwelling fluxes occur where the surface of the cloud is perpendicular to the solar beam. For upwelling fluxes, horizontal photon transport causes the field to diffuse. In some localized areas, the broadband albedo appears greater than unity due to multiple scattering at cloud edges and 3-D effects. Gases are the dominant absorbers, but the high peaks at the cloud edges mask the overall gaseous absorption and shadowing by clouds reduces gaseous absorption in the lower part of the atmosphere. Multiple scattering at cloud edges enhances photon pathlengths, causing increase absorption by gases. The maximum absorption by droplets occurs where the solar beam is perpendicular to the cloud edge. Thus, while the TOA solar irradiance input for the solar zenith angle of 75° (μ = 0.26) is one quarter that of overhead sun, the maximum absorption at 75° is only reduced by about one third. For non-overhead sun, large horizontal gradients in heating rates are observed with differences of more than 1° K hr $^{-1}$ occurring over distances of a few hundred meters. Calculation of longwave fluxes assumes a constant temperature within an atmospheric layer (Fig 3). However, as observed from the previous plot, such an assumption may not be true considering the large variation in heating rates occurring within single layers. The effect of the clear patch in the cloud field can be seen with reduced downwelling infrared radiation near the surface caused by a cooler sky brightness temperature. Rapid cooling is observed at the top of the clouds while heating at the cloud base is caused by the absorption of infrared radiation emitted primarily from the ocean surface.

To examine the variability of the heating and cooling rate profiles, five sampled profiles are plotted in Figure 4. Both the sampled heating and cooling rate profiles are poorly characterized by the domain average profile. At no location does the mean profile match that of an individual column. The maximum average heating rate is less than

0.5° K hr $^{-1}$ while individual columns have heating rates approaching 1.5° K. Generally, these peaks correspond to the individual column's cloud top altitude. However, 3-D effects can also be important. For example, as the sun approaches the horizon the columns heating rates actually increase as the domain average peak decreases. For the chosen cloud field, the use of domain averages or even highly resolved independent column approximations of the radiative fluxes cannot characterize well the actual heating rate of a cloud field. The extent to which the error associated with using a mean profile is propagated into modeling of cloud dynamics needs further examination.

High resolution modeling of cloud fields at TWP site (Wyser, Gautier, Jones, O'Hirok)

Our main objective is to study the capabilities of the Penn State/NCAR mesoscale model (MM5) for regional climate simulations of cloud and radiative properties. The comparison of simulations and data collected at the ARM TWP site during the IOP Nauru99 allows us to estimate the skills of MM5. For this study we use the most recent version 3.3 of the model. The setup of the model and the selected major parameterization are listed in Table 1. The model was run as a nested grid at resolutions of 3,9, and 27 kms.

The model results of the 27 km domain are first compared against GMS-5 images, where the 5 km satellite images have been re-sampled at 25 km. The cloud cover of MM5 is defined as the fraction of area grid-points where cloud water exceeds 5 g/m^2. The GMS visible albedo is converted to cloud cover by dividing all pixels with albedo exceeding 20% by the total number of pixels in the area under consideration. Figure 5 compares the cloud cover of the model against satellite observation. Agreement is poor if the cloud cover of GMS is evaluated in an area of equal size as the model's domain 1. This is not too surprising: The area covered by domain 1 is compared to the scale of cloud systems in the Western Pacific and the cloud cover is highly sensitive to the location of the domain. A slight displacement of the boundary can have a large effect upon the derived cloud cover. A better agreement is achieved if the area of the satellite image is extended to cover about four times the size of domain 1, The larger area is more representative for climatological values at the cost of reduced variability.

Second, the model results were compared to upper air radio soundings from Nauru made every 6 hours during the first 7 days of integration and 3 hours thereafter. These upper air observations (BBSS) were compared against profiles extracted from MM5 at the nearest grid-point approximately 30 minutes after the radiosonde has been released. The difference between these observational profiles and the simulation is shown in Figure 6. It seems that neither the different microphysical schemes nor the variation of the resolutions have much impact on the results.

There are, however, a few systematic differences between model results and observations. The model generally overestimates the tropopause temperature and underestimates the temperature at the top of the boundary layer.

Finally, model results were compared to observations of pressure, temperature and humidity at Nauru (SMET) are compared against model results in the nearest grid-point (Fig. 7). The simulated surface (SFC) pressure does exceed the observed, but it shows a similar 12-hr fluctuation--though the modeled amplitude is not large enough in the model. The SFC temperature of MM5 is obtained by adjusting the temperature adiabatically in the middle of the lowest layer (approximately 35 m above ground) to SFC pressure. Figure 7 illustrates that the average SFC temperature is fairly well reproduced while the diurnal variation is largely underestimated by the model. Part of this may be due to the method of computing SFC temperature from the air temperature alone, not taking into account the effects from ground heating or cooling. Another explanation may be the prescribed SST that largely determines the temperature of the lowest model layer. In general, there is little difference in SFC temperature between the various model configurations except for nights during which some of the runs are colder. However, the model runs whose SFC temperature is colder during the night are not always the same.

Differences in humidity between MM5 and observation become apparent in Figure 7. The simulated specific humidity of the lowest layer is compared to the specific humidity derived from reported SFC air and water vapor pressure. The observations show a relatively high level of humidity in the beginning, followed by a dry period culminating during day 7 of the integration and a slightly wetter phase thereafter. The observed specific humidity is not characterized by a diurnal cycle, Instead, the time-scale of the strongest fluctuation is several days. MM5, on the other hand, seems to linger around a more or less constant humidity level, interrupted only for isolated periods of about 24 hours in length with increased humidity. The transition from a humid state in the beginning to a drier state later in the integration is not captured at all by the model. Unlike in the case of temperature and pressure, the differences between model configurations has a larger impact on the specific humidity of the lowest layer, but these differences do not seem to be systematic in nature.

Besides comparing standard meteorological variables we take advantage of some of the additional observations collected by Atmospheric Radiation and Cloud Station (ARCS-2) in Nauru. The microwave radiometer (MWR)

provides information about vertically integrated humidity (Q_{tot}) and cloud water (LWP). Radiometers measure broadband downwelling SW and LW radiation (SKYRAD) that can be compared to the output of the radiation scheme in MM5. Finally, information about clouds is derived from Vaisala ceilometer data (VCEIL). The cloud frequency is computed as the fraction of data points with lowest cloud base reported between 0 and 10 km. The mean cloud base altitude is then found by averaging the observed cloud base in these points. The time-averaged values of all these variables together with their respective counterparts from the various model runs are listed in Table 2. MM5 underestimates Q_{tot} irrespective of the microphysical scheme employed, but the inter-model differences are small. In contrast, cloud water varies widely depending on the microphysics, but all values are still lower than the observed average. This large spread between models manifests itself also in the differences in cloud base. The different microphysical schemes control not only where and when clouds form but, equally as important, how they disappear by either generating precipitation or evaporating. These processes affect the distribution of humidity and the subsequent formation of new clouds. This feedback between humidity and clouds accentuates the difference between the various microphysical schemes that only become apparent in longer model runs. Despite the differences in cloud water and base altitude, the frequency of cloud occurrence is more similar and agrees with observations. The lowest frequencies are found when the model is evaluated in the 3 km domain. In both runs with a 3 km domain, the frequency of clouds gets considerably higher if evaluated in the 9 km grid instead. One may conclude that cloudiness is strongly affected by the horizontal resolution of the model, and a more thorough exploration of cloudiness and its definition is required.

The effect of surface albedo Heterogeneity on sky radiance (Ricchiazzi, Payton, Gautier)

Since about 1987 the Antarctic Monitoring System, sponsored by the National Science Foundation, has been gathering high resolution UV radiation spectra from three sites in Antarctica: South Pole, McMurdo and Palmer. The observations from Palmer Station are especially interesting because of its proximity to a highly productive marine ecology that could be stressed by the enhanced levels of UV radiation that occur in the austral spring. UV observations from Palmer provide the best long-term dataset with which to assess how ozone depletion affects bio-productivity of the Southern Ocean.

Downwelling radiation over a highly reflecting surface is increased by multiple reflection between the surface and sky, especially when clouds are present. Several previous studies have documented this effect in regions of uniform surface reflectivity However, less is known about the level of increase expected near an abrupt transition in surface albedo, such as found at Palmer Station, a high-latitude coastal site which is often free of ocean ice in the spring and early summer. It is important to quantify how non-homogeneous surface reflectance impacts the interpretation of the Palmer UV data.

During a field campaign conducted at Palmer Station during the Spring of 1999, we observed sky radiance with an all-sky camera and an Analog Spectral Devices spectroradiometer. The measured radiance values for several cloudy and one clear sky day were compared to results from a 3-D Monte-Carlo radiation model that explicitly includes the interaction of radiation with heterogeneous surface features. Calculations were performed at the MFRSR wavelengths (414, 500, 609 ,665 and 861 nm), and for cloud optical depths of 15 and 30.

Figure 8 shows the normalized radiance (radiance divided by zenith radiance) predicted by the model for the 414 and 861-nm channels, and for cloud optical depth 15 and 30. The model computations predict that the level of sky radiance enhancement over the glacier is wavelength dependent due to the spectral variation of snow reflectivity. For the optical depth 30 case, the enhancement is about 30% for the 414-nm channel, but only 20% for the 861 nm channel. In the sea-ward direction the normalized radiance is essentially the same for the two channels.
The ASD spectral observations for 20nov99 are shown in Figure 9. The sky radiance increases for all wavelengths as the viewing angle is scanned from the SW through the zenith and to the NE (except for the strong absorption in the Oxygen A band). The lower plot in Figure 8 shows a comparison of the observed normalized radiance with the Monte Carlo results. The computed radiance for thin (diamonds) and thick (triangles) clouds brackets the observations for each viewing direction. In addition, the downward trend with wavelength of the 60NE (toward glacier) scan seems to be well reproduced in the simulation.

Overall, the results for 1dec99 (Figure 10) do not agree as well. Though the match is fairly good in the SW direction, the normalized radiance is much greater than the model predictions in the NE direction. Furthermore, the constancy of the normalized radiance with wavelength over the glacier (60NE) is inconsistent with the model calculations. For the conditions on this day, it appears that multiple reflection between the cloud and glacier does not decrease radiance levels toward the red and near-IR as it does for the 20nov99 case. This may be due the nature of the cloud layer, which, according to the all-sky image, has much greater horizontal structure than for 20nov99.

Spectrally resolved spectrometer data in conjunction with RT model computations

The SSFR developed by the SGP Radiation Group has been used to measure spectral solar irradiance at moderate resolution to determine the radiative impact of clouds, aerosols, and gases on climate, and also to infer the physical properties of aerosols and clouds. In the Spring of 1999 the SSFR was used to obtained detailed moderate resolution solar spectral measurements as part of the SHEBA campaign.

We have generated a CK database for the SSFR in 0.255 to 1.00 μm spectral region using a sensor filter function specific to the instrument deployed at the SHEBA site. The normalized spectral response function (SRF) (private communication, Peter Pilewskie, 2000) has 85 points at intervals of 0.25 nm. The SRF is a skewed Gaussian, extending 4 nm from peak wavelength toward the blue and 17 nm toward the red. The CK database of SSFR extends from 0.26 to 1.0 μm with 5 nm steps, and a total 150 spectral channels. The bandwidth of each channel is 0.021 μm. Preliminary comparisons between observations and model results indicate a close agreement, except in the mid-visible here the difference can be large and might be explained by the solar spectrum used in the computations.

	Domain 1	Domain 2	Domain 3
Gridsize	44×44	64×64	115×115
Resolution	27 km	9 km	3 km
Timestep	90 s	30 s	10 s
Convection	Grell (1993)	Explicit	Explicit
Boundary layer	MRF (Hong and Pan (1996))		
Microphysics	Schultz (1995) / Reisner (1998) / GSFC (Tao and Simpson (1993))		
Radiation	CCM2 (Kiehl et al., 1994), updated every 30 minutes		
Vertical setup	σ-coordinate sytem, 23 layers, rigid lid at 50 hPa		

Table 1 Model setup

	Qtot (kg/m2)	LWP (g/m2)	Swdown (W/m2)	Lwdown (W/m2)	Cloud base (m)	Cld frequency (%)
Obs	47.7	140.2	212.8	415.1	1350	27
GSFC 2_2	43.4	63.4	263.2	409.8	1078	38
Reisner 2_2	43.2	43.2	237.7	419.5	905	36
Reisner 3_2	43.2	23.3	280.9	409.8	839	39
Reisner 3_3	43.2	23.6	269.0	411.4	671	22
Schultz 2_2	43.2	38.7	213.7	420.5	811	37
Schultz 3_2	42.9	14.3	257.6	411.7	751	37
Schultz 3_3	42.9	11.9	242.3	401.1	822	16

Table 2 Model comparison with observations for MWR (Q_{tot} and LWP), SKYRAD (SW_{down} and LW_{down}), and VCEIL (Cloud base and frequency of occurrence), only the mean values are listed. The average cloud base altitude has been calculated for cloudy conditions only.

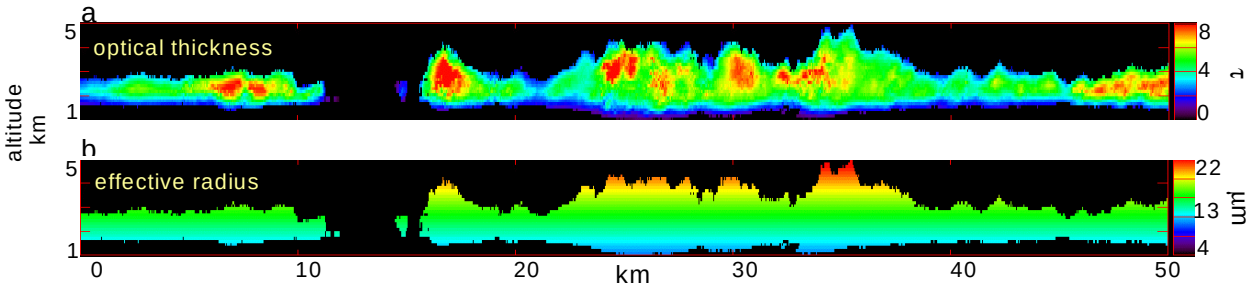

Figure 1. (a) Optical thickness and (b) cloud droplet effective radius for model cloud input.

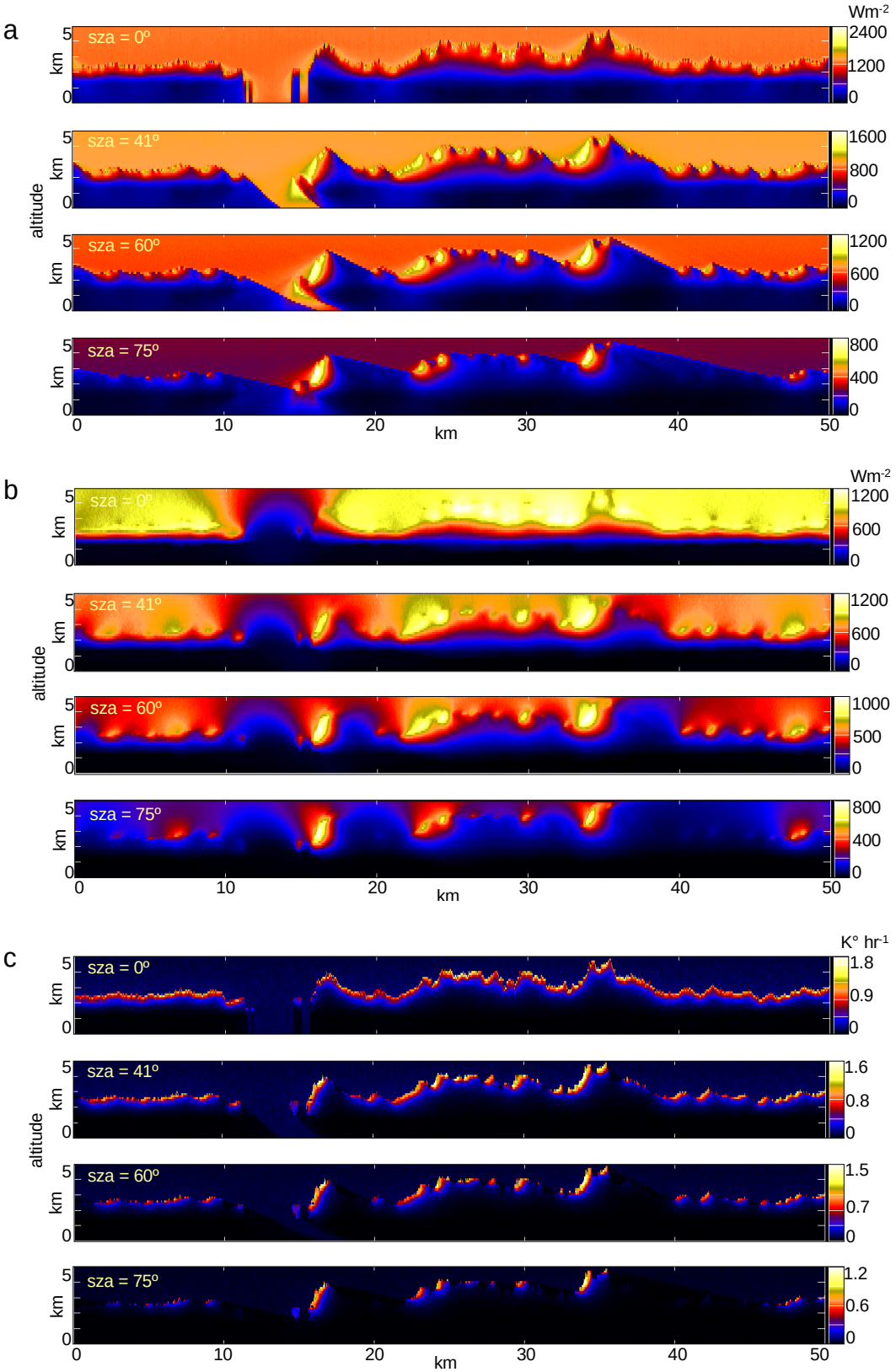

Figure 2. (a) Upwelling and (b) downwelling solar irradiance, and (c) heating rates for solar zenith angles of 0, 41, 60 and 75 degrees.

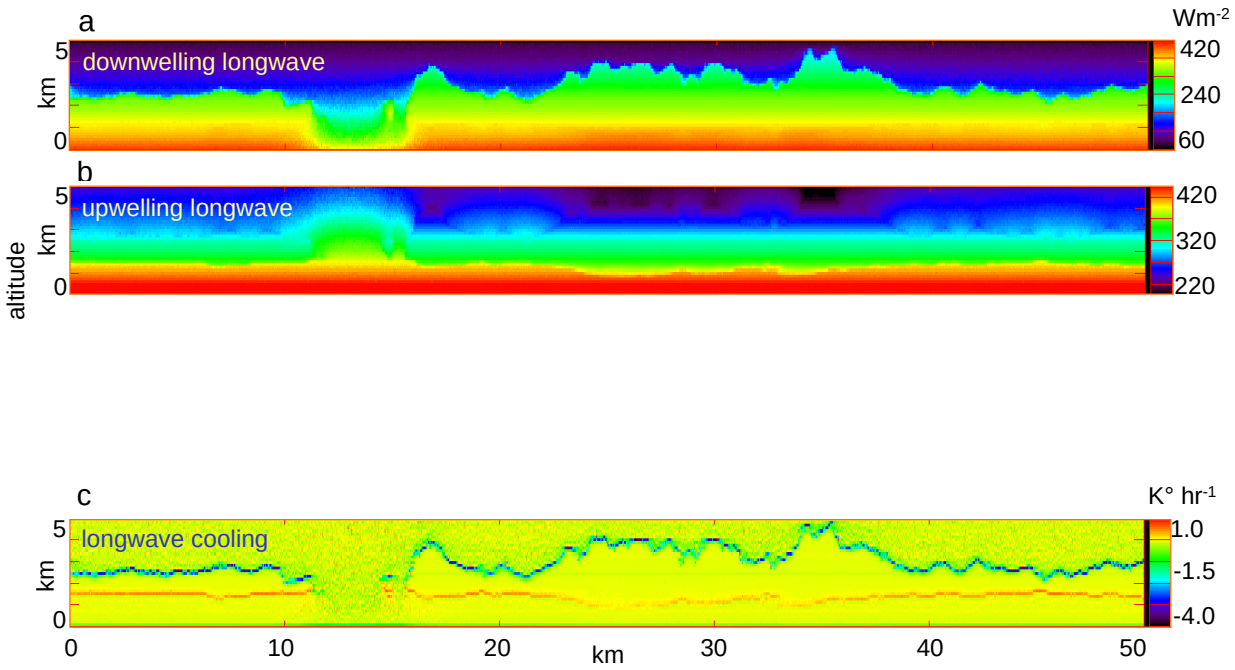

Figure 3. (a) Upwelling and (b) downwelling longwave fluxes, and (c) cooling rates.

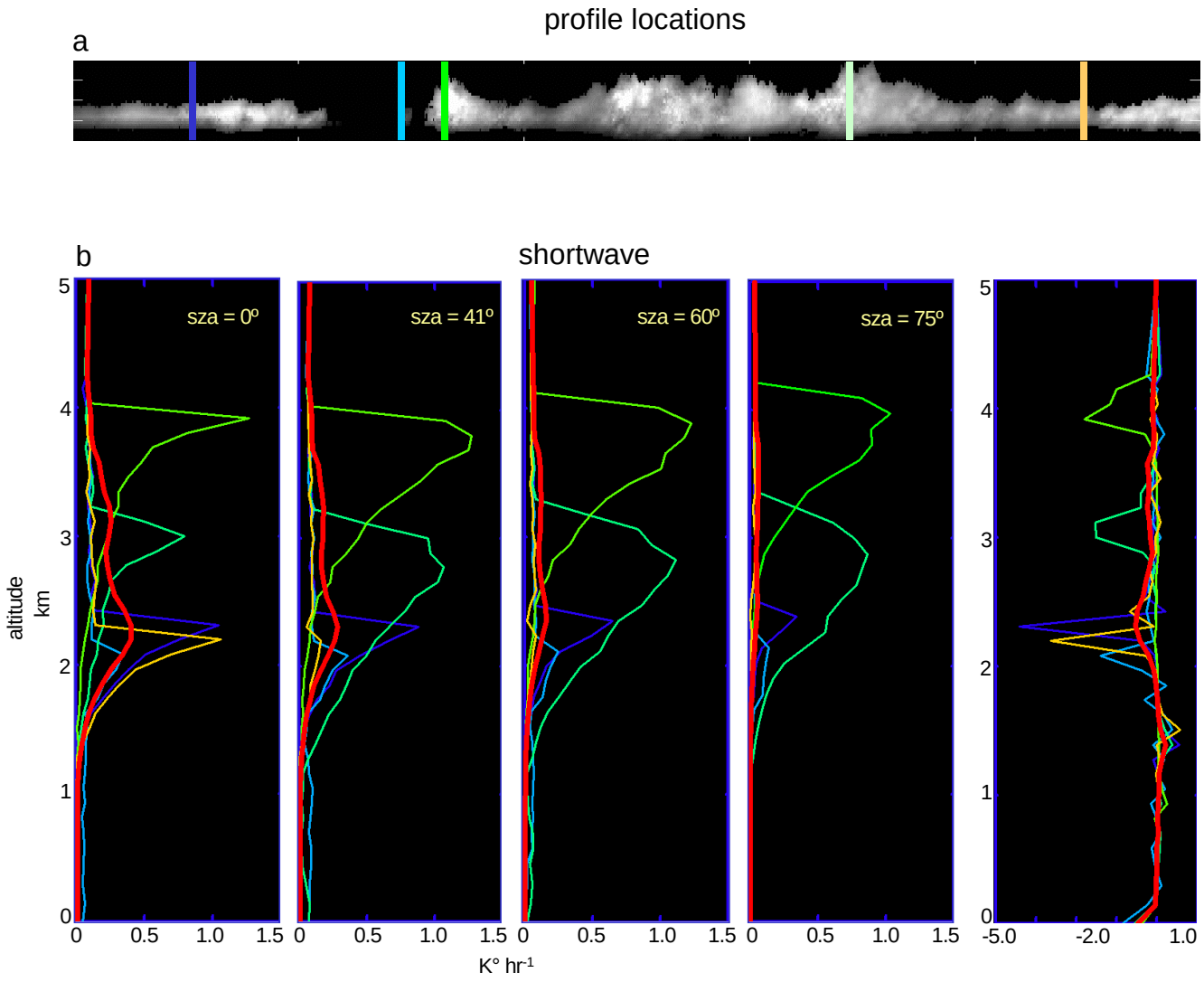

Figure 4. (a) Location of profile samples. Color bars match selected profiles. (b) Heating and cooling rate profiles for sampled locations.

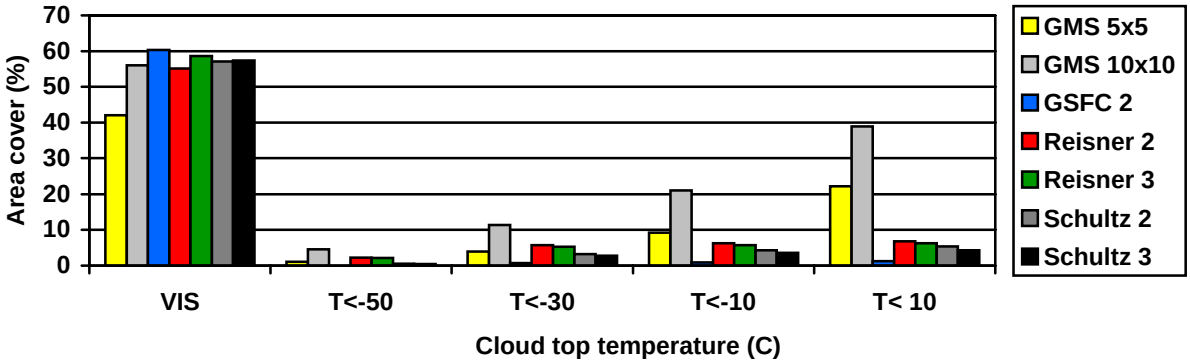

Figure 5 Cloud cover comparison between MM5 in domain 1 and GMS-5, visible and IR channels. GMS cloudiness is evaluated in a 5°×5° and a 10°×10° domain. The different model runs are identified by their microphysical scheme, the number denotes the number of domains used in the simulation, for example, "Schultz 2" is a run with Schultz' microphysics with the 27 and 9 km domains.

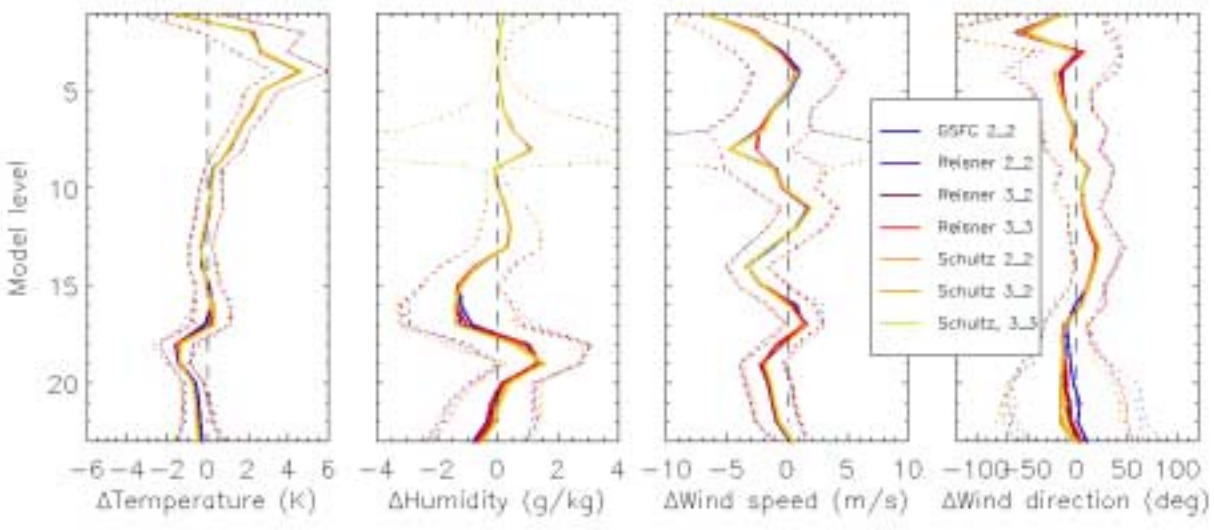

Figure 6 Averaged difference between MM5 profile in nearest gridpoint to Nauru and the radiosounding (BBSS) from Nauru. The different runs are identified by the name of the microphysical scheme, followed by the number of domains in the simulation and the resolution at which the variable is evaluated, for example "Schultz 3_2" is a run with the Schultz scheme and all 3 domains but the variable is evaluated on the 9 km grid.

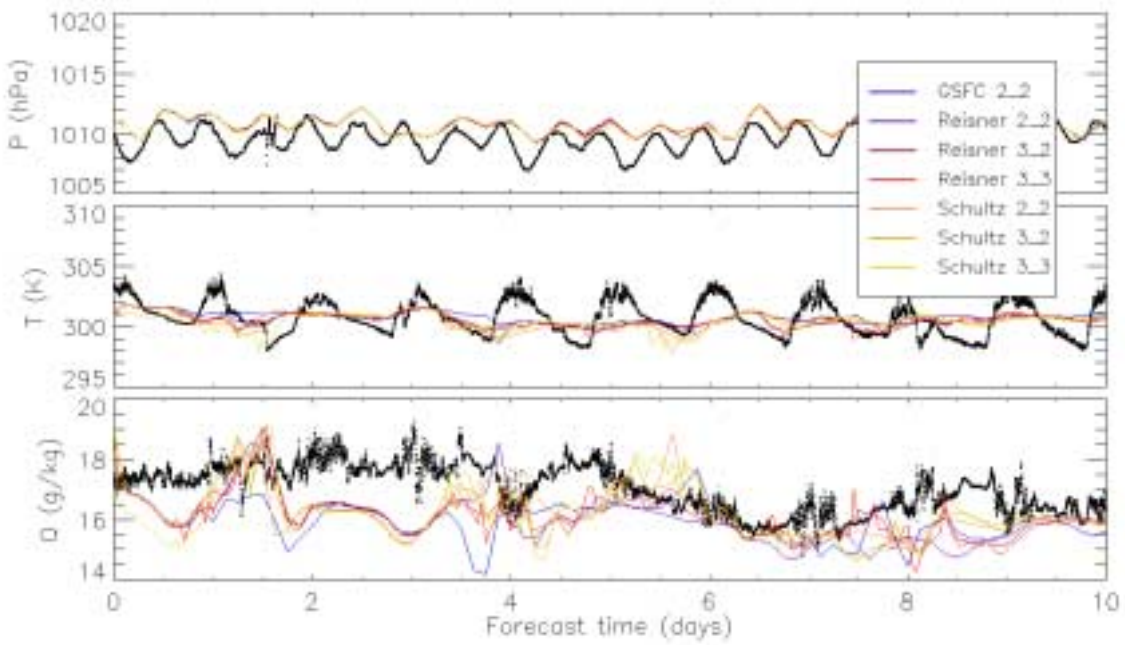

Figure 7 Time series of SFC observations (black dots) and MM5 variables at nearest gridpoint, same naming convention as in Fig. 6.

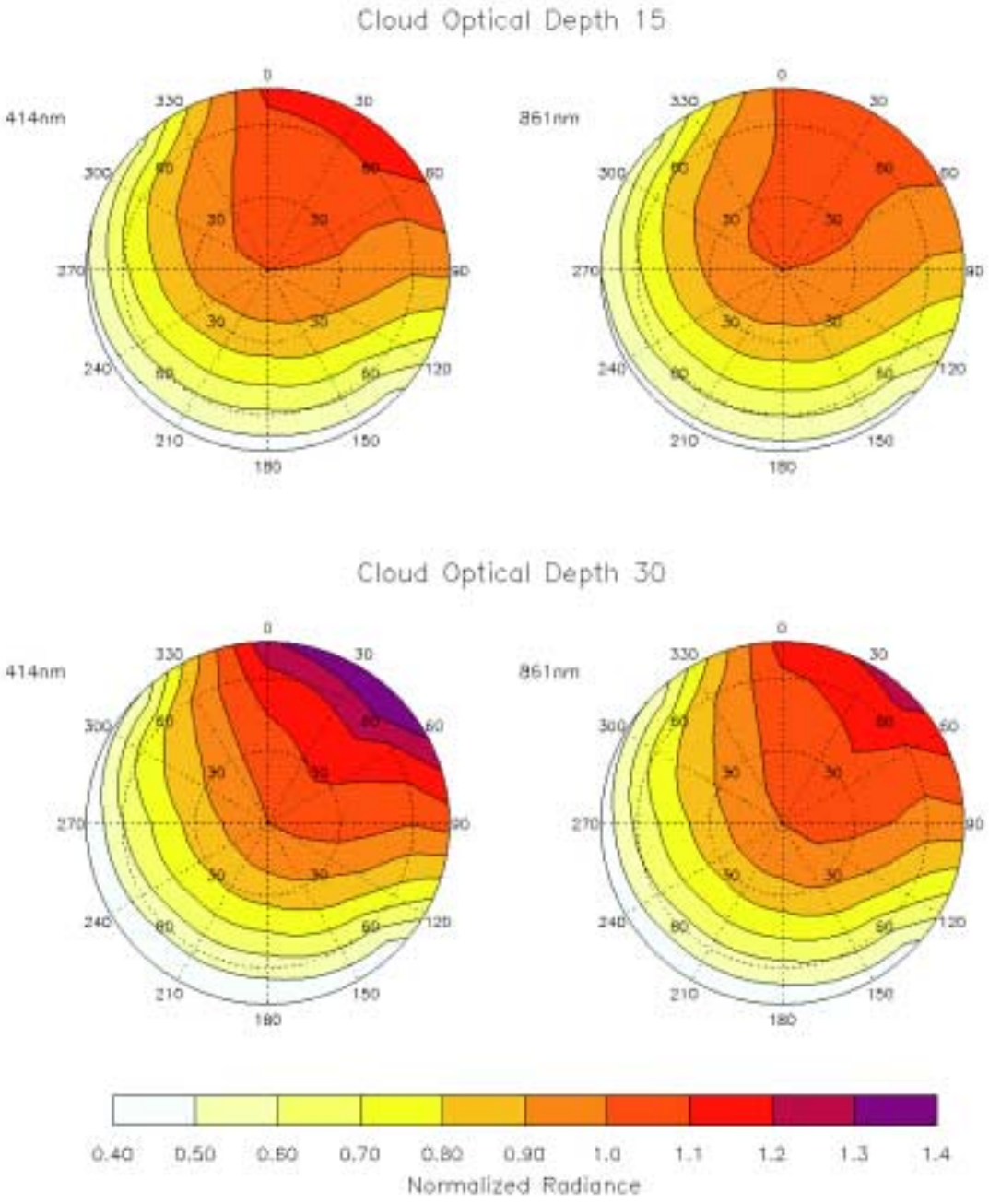

Figure 8. Computed 3-D radiance distribution for the 414 and 861-nm channels, for cloud optical depth 15 and 30. The glacier is to the North-East.

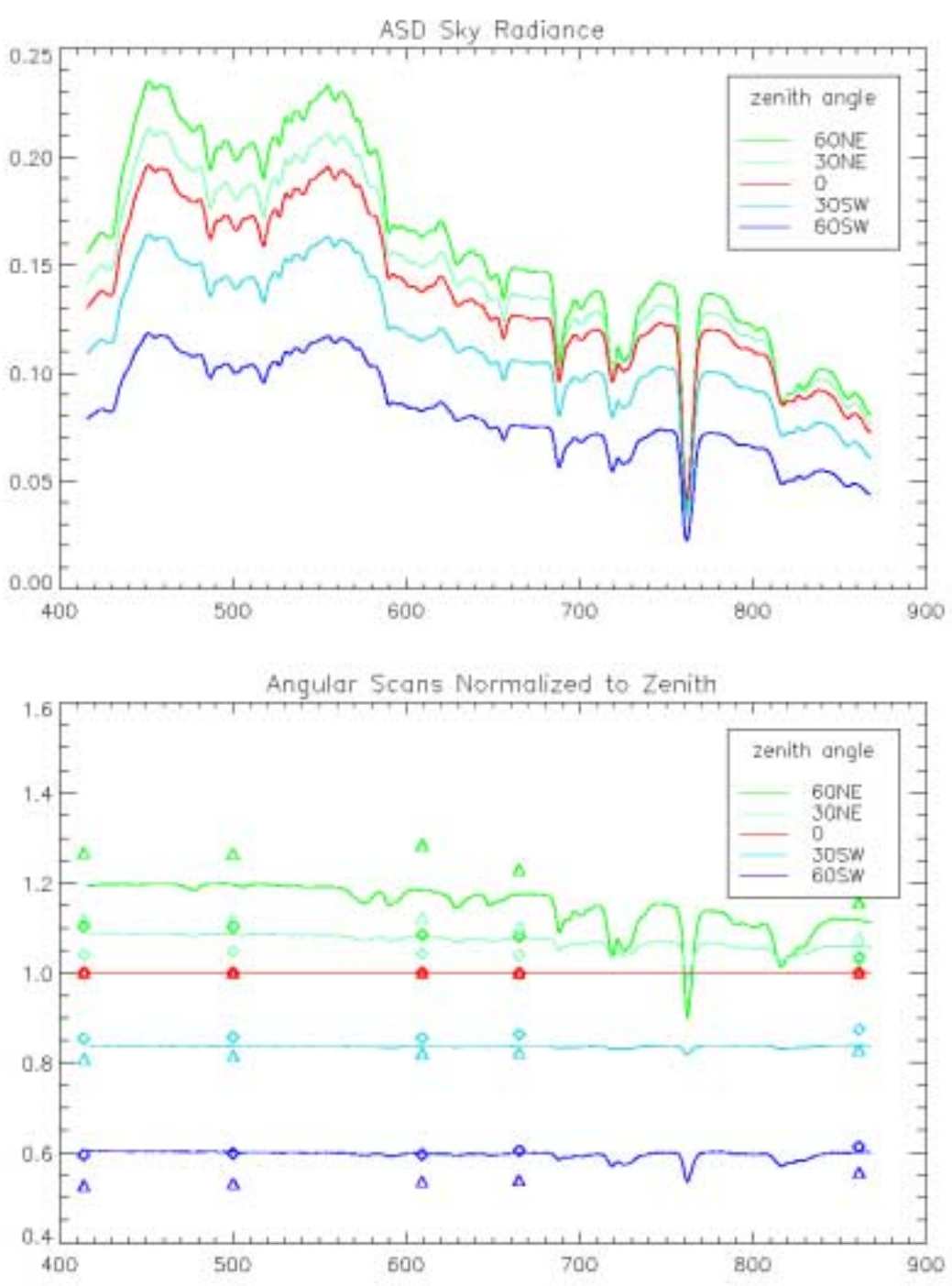

Figure 9. ASD radiance scan for 20nov99 (upper). Radiance at each viewing angle normalized to the zenith radiance is shown in the lower panel. Computed results are shown as diamonds (t = 15) and triangles (t = 30).

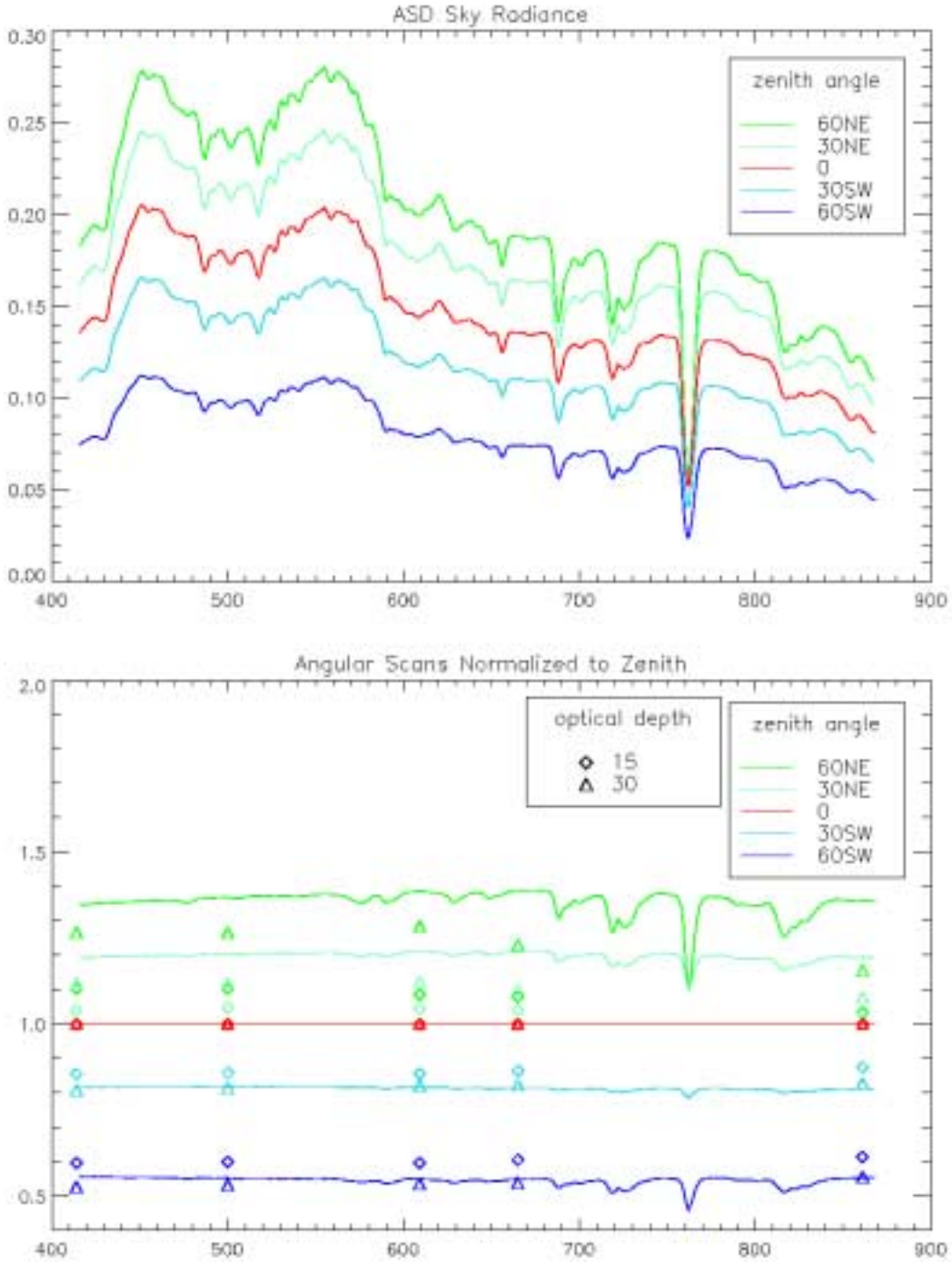

Figure 10. Same as Figure 9 for 1dec99.

7-8. Publications and extended abstracts

Gautier, C., W. O'Hirok and P. J. Ricchiazzi, 1999: "Potential physical processes explaining the observed spectral signature of cloudy column solar radiation absorption," Proceedings of the 10th Conference on Atmospheric Radiation: A symposium with tributes to the works of Verner E. Suomi, Madison, WI, 28 June-2 July 1999, p 455-458.

Gautier, C., and P. J. Ricchiazzi, 1999: "A possible process enhancing absorption of shortwave radiation in cloud-free conditions," Proceedings of the 10th Conference on Atmospheric Radiation: A symposium with tributes to the works of Verner E. Suomi, Madison, WI, 28 June-2 July 1999, p 451-454.

Gautier, C., S. Yang and P. J. Ricchiazzi, 1999: "A moderate spectral resolution radiative transfer model for remote sensing of cloud and atmospheric properties," Proceedings of the 10th Conference on Atmospheric Radiation: A symposium with tributes to the works of Verner E. Suomi, Madison, WI, 28 June-2 July 1999, p 189-192.

Gautier, C., W. O'Hirok and K. Wyser, 1999: "Remote sensing of surface solar irradiance: corrections for 3-D cloud effects," Proceedings of the EOS/SPIE Symposium on Remote Sensing, 20-24 September, Florence, Italy.

O'Hirok W., and C. Gautier, 1999: "Potential biases in remotely sensed cloud properties due to the plane parallel cloud assumption employed in retrieval algorithms," Proceedings of the EOS/SPIE Symposium on Remote Sensing, 20-24 September, Florence, Italy.

Gautier, C., S. Yang and P. J. Ricchiazzi, 1999: "Cloud and Aerosol Remote Sensing Using a New Radiative Transfer Model: Application to MODIS," Proceedings of the EOS/SPIE Symposium on Remote Sensing, 20-24 September, Florence, Italy.

Yang S., P. J. Ricchiazzi and C. Gautier, 2000: Modified correlated-k distribution methods for remote sensing applications," *Journal of Quantitative Spectroscopy and Radiative Transfer (JQSRT),* vol. 64:585-608.

O'Hirok W. and C. Gautier, 2000: "High Resolution Heating and Cooling Rather in 3-D Clouds," Extended abstract, Tenth Atmospheric Radiation Measurement Science Team Meeting, San Antonio, TX, March 2000.

Wyser K. , C. Gautier , C. Jones, and W. O'Hirok, 2000: "High Resolution Modeling of Cloud Fields at the TWP Site with MM5," Extended abstract, Tenth Atmospheric Radiation Measurement Science Team Meeting, San Antonio, TX, March 2000.

Gautier, C. Paul Ricchiazzi, and A. Payton, 2000: **"**The Effect of Surface Albedo Heterogeneity on Sky Radiance," Extended abstract, Tenth Atmospheric Radiation Measurement Science Team Meeting, San Antonio, TX, March 2000.

Gautier, C. W. O'Hirok, and P. J. Ricchiazzi: "Spectral signature of column solar radiation absorption during ARESE," *Journal of Geophysical Research (Atmospheres)* (in-press).